Impact of extreme CO_2 levels on tropical climate: A CGCM study

Annalisa Cherchi[1,2], Simona Masina[1,2], and Antonio Navarra[1,2]

[1]Centro Euro-Mediterraneo per i Cambiamenti Climatici, Bologna, Italy
[2]Istituto Nazionale di Geofisica e Vulcanologia, Bologna, Italy

Manuscript submitted to

Climate Dynamics

March 27, 2008

Abstract

A coupled general circulation model has been used to perform a set of experiments with high CO_2 concentration (2, 4, 16 times the present day mean value). The experiments have been analyzed to study the response of the climate system to strong radiative forcing in terms of the processes involved in the adjustment at the ocean-atmosphere interface. The analysis of the experiments revealed a non-linear response of the mean state of the atmosphere and ocean to the increase in the carbon dioxide concentration. In the $16xCO_2$ experiment the equilibrium at the ocean-atmosphere interface is characterized by an atmosphere with a shut off of the convective precipitation in the tropical Pacific sector, associated with air warmer than the ocean below. A cloud feedback mechanism is found to be involved in the increased stability of the troposphere. In this more stable condition the mean total precipitation is mainly due to large-scale moisture flux even in the tropics. In the equatorial Pacific Ocean the zonal temperature gradient of both surface and sub-surface waters is significantly smaller in the 16xCO2 experiment than in the control experiment. The thermocline slope and the zonal wind stress decrease as well. When the CO_2 concentration increases by about two and four times with respect to the control experiment there is an intensification of El Niño. On the other hand, in the experiment with 16 times the present-day value of CO_2, the Tropical Pacific variability weakens, suggesting the possibility of the establishment of permanent warm conditions that look like the peak of El Niño.

1 Introduction

The XX century has been characterized by an increase of the global mean temperature, as reported from the Intergovernmental Panel on Climate Change (IPCC, 1995, 2001). The general warming has been mainly attributed to the increase of the greenhouse gases (GHGs) concentration of the last decades. In the atmosphere, the increase in CO_2 concentration and the associated increase in global temperature is accompanied by an increase in water vapor concentration both at low and high levels (Trenberth et al., 2007). When the surface warms, the water vapor concentration in the lower troposphere increases consistently with the Clausius-Clapeyron equation and fixed relative humidity (e.g. Manabe and Wetherald, 1967; Held and Soden, 2006).

The concept of climate sensitivity, defined as a measure of a model's temperature feedback to external radiative forcing (IPCC, 2001), assumes that climate response is approximately proportional to radiative forcing. However, yet not much is known about the range of forcing under which such a view is reasonable. Strong radiative forcing applied to a global coupled climate model suggested the possibility of a runaway greenhouse effect, with the climate system far from an equilibrium in the neighbourhood of the current climate (Boer et al., 2005). Furthermore, climate response to strong forcing regimes may also represent a framework for the development of some paleoclimate applications.

The regulation of the tropical climate involves the coupling between large-scale circulation and local environment (Wallace, 1992; Pierrehumbert, 1995) as well as the ocean dynamics (Clement et al., 1996). However, changes in shortwave cloud forcing, through the thermostat mechanism (Ramanathan and Collins, 1991, 1992) and evaporation (Wallace, 1992) are negative feedbacks efficient in limiting SSTs in the warm pool region. In the Equatorial Pacific Ocean the interaction between convection and large-scale circulation is needed to explain the relationship between latent heat flux and SST (Zhang and McPhaden, 1995). Among the IPCC AR4 assessment, water vapor has been identified as the largest positive feedback acting in future climate change scenarios (Soden and Held, 2006).

Changes in the distribution of the large-scale heating could substantially affect the large-scale extra-tropical, as well as the tropical, circulation (Knutson and Manabe, 1995). Observations trends as well as model projections evidenced a weakening of the Walker circulation due to anthropogenic forcing increase (e.g. Houghton et al., 2001; Vecchi et al., 2006), thus reducing the strength of the mean tropical atmospheric circulation.

In the tropics, a weakening of the Walker circulation has been found to be associated with an

eastward shift of convection over the central equatorial Pacific, a reduction of the sea level pressure (SLP) gradient across the equatorial Pacific and of the tilt of the equatorial Pacific thermocline, a shoaling of the thermocline depth in the western Pacific, a preferential warming of SST along the eastern equatorial Pacific and a weakening of equatorial easterlies, suggesting that a warmer climate may be associated with reduced zonal gradient conditions (Vecchi and Soden, 2007). However, the climate conditions induced by an increase in CO_2 differs from El Niño pattern as the warming occurs both in the tropics and extra-tropics and precipitation is increased throughout the tropics (Knutson and Manabe, 1995). In increased CO_2 conditions an enhanced equatorial warming relative to the sub-tropics associated with surface latent heat flux, shortwave cloud forcing and surface ocean mixing represents a robust fingerprint to global warming (Liu et al., 2005).

A number of modeling studies revealed that doubling and quadrupliying CO_2 concentration experiments produce an El Niño with a preferred period of 2 years (Knutson and Manabe, 1995; Collins, 2000; Meehl et al., 2001). Nevertheless, the analysis of ENSO in a changing climate by means of XX century and future climate scenario experiments revealed contradictory results about the changes in the El Niño frequency (Capotondi et al., 2006; Meehl et al., 2006; Guilyardi, 2006; Merryfield, 2006).

The understanding of the processes involved in the climate feedback/sensitivity is crucial to gain confidence in climate change simulations at any forcing levels (Boer et al., 2005). With the aim to investigate the response of the climate system to strong forcing in terms of its linearity and of the feedbacks involved in the ocean-atmosphere adjustments, the SINTEXG CGCM (Gualdi et al., 2007) has been used to build experiments with modified CO_2 conditions. The carbon dioxide concentration has been multiplied by a factor of 2, 4 and 16 with respect to the value used in a control simulation. The analysis performed represents a link between studies focused on the changes of mean climate to CO_2 scenarios (e.g. Vecchi and Soden, 2007) and studies on the response to extreme radiative forcings (e.g. Boer et al., 2005). Specific emphasis has been dedicated to the mean state and variability of the tropical Pacific sector.

The study is organized as follows: section 2 briefly presents the model used and the experiment performed. Section 3 describes the main changes of the mean state of the tropical climate induced by the CO_2 increase introduced in the experiments. Section 4 focuses on the mechanisms involved in the ocean-atmosphere adjustment to explain the changes described in the Tropical Pacific sector. Section 5 describes the changes occurring in the simulation of the Tropical Pacific variability. Finally, section 6 collects the main conclusions of the study.

2 Model experiments and observational datasets

The CGCM used in this study is SINTEXG (Gualdi et al., 2007). It represents the new generation of the SINTEX CGCM (Gualdi et al., 2003; Guilyardi et al., 2003) where the ocean model is coupled to a sea-ice model. The atmospheric component is Echam4.6, which is parallelized through the MPI interface. It represents the 4^{th} generation of the ECHAM model developed at the Max-Planck Institute für Meteorologie in Hamburg. The resolution used for this analysis is a spectral T30 horizontal resolution with $3.75^{\circ} \times 3.75^{\circ}$ grid-points and 19 vertical sigma levels. A detailed description of the physics implemented within the atmospheric model is shown by Roeckner et al. (1996).

The oceanic component is OPA8.2 (Ocèan PAralelisée), the global ocean general circulation model developed at LODYC in Paris (Madec et al., 1998). It is a primitive equation model. The prognostic variables are the three dimensional velocity field and the thermohaline variables. The distribution of the variables is over a three-dimensional Arakawa-C-type grid and 31 prescribed vertical levels. The spatial resolution is about $2^{\circ} \times 2^{\circ}$, with a meridional resolution of 0.5° at the Equator. Vertical eddy diffusivity and viscosity are computed from a 1.5 closure scheme which allows an explicit formulation of the mixed layer as well as minimum diffusion in the thermocline (Blanke and Delecluse, 1993).

The OPA OGCM includes the LIM (Louvain-laneuve sea-Ice systeM) module for the interactive ice. The LIM model has been developed at the "Institut d'Astronomie et de Geophysique Georges Lemaître" (Université Catholique de Louvain). It is a large-scale thermodynamic-dynamic sea-ice model with 3-layers (one for the snow and two for the ice). The details of the model equations and parameterizations are described by Fichefet and Morales Maqueda (1999).

The atmospheric and oceanic components are coupled with Oasis2.4 (Valcke et al., 2000). The air-sea fluxes and the SST are exchanged every 3 hours. No flux corrections are applied to the coupled model.

A long (300 years of integration) control experiment (CTRL) has been analyzed and compared with several sensitivity experiments with modified CO_2 conditions. In particular, the carbon dioxide concentration of the control experiment (mass mixing ratio = 353 ppmV) has been multiplied by a factor of 2, 4 and 16 to build 2xCO2, 4xCO2 and 16xCO2 experiments, respectively. There is no gradual ramp up of the forcing in the experiments, as the CO_2 increase is applied at the beginning. The 16xCO2 experiment is 350 years long, while the 2xCO2 and 4xCO2 experiments are 200 years long, and in all of them only the last 100 years are used for the analysis.

The coupled model experiments results have been compared with observational datasets, when available, or with atmospheric reanalysis and ocean analysis. The net surface heat flux is taken from the observed climatology available from Da Silva et al. (1994). The SST field is taken from the HadISST dataset (Rayner et al., 2003); while the vertical distribution of the ocean temperatures comes from an ocean analysis (Masina et al., 2004).

3 Impact of increased CO_2 on ocean and atmosphere mean state

The oceans are governed by a balanced heat budget, which is controlled by the heat transport and the heat fluxes at their surface.

The annual mean heat budget at the ocean surface is shown in fig. 1. It has been computed by adding the net surface short wave radiation (SWR), the net surface long wave radiation (LWR), the net surface latent heat flux (LHF) and the net surface sensible heat flux (SHF) over the ocean grid points. From the observed climatology (fig. 1a), the main regions of ocean heat loss to the atmosphere are located near the western boundary currents, where the oceans lose heat when cold dry winds from the continent blow over the warm waters carried by the currents. The main areas of heat gain are located over the tropical bands of the Pacific and Atlantic Oceans along the eastern boundary of the ocean basins (fig. 1a). They correspond to up-welling regions where relatively cold SST does not allow evaporation to balance insolation resulting in a net heat gain. In the control experiment the features described are realistically simulated (fig. 1b), even if some biases are present. In particular, the coupled model tends to have less heat loss in the sub-tropics regions in both hemispheres, and the region of heat gained at the Equator extends too westward with respect to the observations. The last feature is a consequence of the bias in the simulation of the cold tongue regime of the SINTEXG coupled model, which was present even in the previous version of the model (Gualdi et al., 2003). The differences between the perturbed CO_2 experiments and the control experiment reveal that as the CO_2 concentration increases there is a drastic decrease of heat loss near the western boundary currents (fig. 1c-d). In the 16xCO2 experiment the heat gain decreases at the Equator, while it increases in the band along 10°N (fig. 1e). In the Atlantic sector, the 16xCO_2 experiment (fig. 1e) has more heat gained at the Equator and less heat loss in the northern latitudes along the western boundary (i.e. 40°N). In the Equatorial Indian Ocean, the departures from the control simulation are positive in the west and negative in the east (fig. 1d-e).

Each component of the surface heat budget has been analyzed as well. The computation of the global ocean average for each component reveals that an increase in the CO_2 concentration

is accompanied by a decrease of short wave radiation, a decrease of the lost long wave radiation, a decrease of the sensible heat flux and an increase of the latent heat flux. The changes in the radiation fluxes are mainly linked to the changes in the cloud cover fraction distribution at low and high levels. Indeed, in the tropics, the cloud cover fraction increases at low levels and decreases at high levels (fig. 2). On the other hand, the changes in the latent heat flux as well as the changes in the sensible heat flux are related to changes in the balance between evaporation, moisture and air-sea temperature gradient occurring at the surface.

The zonal net surface heat fluxes averaged over the global ocean (fig. 3a) evidence a decrease in heat gain at the equator together with a decrease of heat loss in the northern extra-tropics. At the Equator, most of the decrease in heat gain is a contribution from the Pacific Ocean where the zonal SST gradient is reduced in the 16xCO2 experiment with respect to the control simulation (see also the discussion in the next section). On the other hand in the northern hemisphere extra-tropics the main contribution to the decreased heat loss is given by the Atlantic Ocean (not shown). The changes described in the surface heat fluxes are consistent with a changed ocean heat transport (fig. 3c). In fact, in the northern extra-tropics the decrease of heat loss is associated with a decreased poleward heat transport, particularly in the North Atlantic. The poleward ocean heat transport works as a negative feedback on the SST gradient between low and high latitudes. The Equator to pole SST gradient in the northern hemisphere increases of about 1° and 2°C in the 2xCO2 and 4xCO2 experiments respectively, while it decreases of about 1°C in the 16xCO2 experiment (fig. 3b). In the atmosphere (fig. 3d) the main differences in the meridional heat transport (computed as $\left[\overline{vT}\right]$, where the square brackets refer to the zonal average, while the overbar indicates the time mean) between 16xCO2 and control experiments occur in the tropical sector. In fact, the thermally direct Hadley cell weakens, providing less poleward heat transport. On the other hand, in the extra-tropics the heat transport, associated with the baroclinic eddies, is almost unchanged.

In the sub-tropics, the surface waters on the west side of the oceans tend to be warmer than those on the east side, whereas at high latitudes the opposite tends to occur (fig. 4a). The coupled model is able to reproduce the main features in a realistic way (fig. 4a,b), with the extra-tropics better simulated than the tropics. Biases are found in the Tropical Pacific Ocean where the warm pool tends to be narrower than observed and the cold tongue extends too westward. Even the Tropical Indian Ocean temperature is biased, as it is colder than observed. An increase in the concentration of CO_2 clearly produces a generalized warming of the surface temperature over the oceans, with the high latitudes which warm more than the tropics (fig. 4). For instance, in the 16xCO2 experi-

ment the ocean temperature increases up to 12°C compared to the control experiment (fig. 4e) in the eastern equatorial Pacific and up to 14°C in the North Pacific. In all the perturbed CO_2 experiments the eastern Equatorial Pacific warms up more than the western side inducing a reduction of the zonal gradient of SST, up to 50% in the 16xCO2 experiment.

As the CO_2 increases, the Indian Ocean warms up homogeneously and the annual precipitation increases up to 4 mm/day in the 16xCO2 experiment (fig. 5). Some continental areas, such as the Amazon basin and the southwestern Africa experience an increase of the precipitation as well. Near the coast of central America the Pacific Ocean experiences a decrease of the annual precipitation. The decrease is even stronger in the open ocean up to the date line. East of the date line, the double Inter Tropical Convergence Zone (ITCZ) weakens, as the main peak of precipitation south of the Equator moves north-westward. In particular, during the summer the double ITCZ simulated by the coupled model in the control experiment completely disappears when the CO_2 is multiplied by a factor of 16 (not shown).

The total precipitation shown in fig. 5 is the sum of convective and large-scale precipitation. In the tropics the main contribution is given by the convective precipitation, while the large-scale precipitation is higher in the extra-tropics. In the control experiment, this distinction is clear, but when the CO_2 concentration increases their relative role changes. For instance, in the 16xCO2 experiment the large-scale precipitation in the Pacific Ocean in the band 15°S-15°N increases by about 4 mm/day (not shown), while the convective component decreases by about 2 mm/day (fig. 6). Over land (e.g. in the Equatorial Africa and in the north-western Brazil) as the CO_2 increases the convection tends to increase, probably because the land warms quickly and tend to remain warmer than the air above.

At the surface, in the tropical band between 15°S-15°N, the ocean is generally warmer than the air above it (fig. 7). The positive gradient between SST and air temperature enables the loss of sensible heat from the surface, and represents a requisite for convection to occur. In the coupled model experiments, as the CO_2 concentration increases the Equatorial Pacific Ocean experiences a gradual change of the sign of the SST-air temperature gradient (fig. 7). In the 16xCO2 experiment the Equatorial Indian, Pacific and Atlantic Oceans have SSTs which are colder than the air above up to 0.8°C in the western equatorial Pacific Ocean. In this condition the sensible heat lost from the surface changes sign and convection is shut off as also revealed by the decrease of the convective component of precipitation (fig. 6). In this condition, precipitation is mainly linked to the large-scale convergence of moisture flux. In the same region, the latent heat flux released from the ocean increases, consistently with an increased evaporation rate. The amount of evaporation and

hence the latent heat flux depend on the difference between the saturated vapor pressure over sea water and the actual vapor pressure in the air above sea. Warmer surface temperatures increase the saturation vapor pressure following the Clausius-Clapeyron equation and evaporative processes persist until the saturation is reached.

In increased CO_2 conditions, the whole troposphere tends to be more stable. In particular, in the Tropical Pacific Ocean an increase in the carbon dioxide concentration is accompanied by a tropospheric warming (fig. 8). From the figure it seems that as the CO_2 concentration increases the tropopause becomes higher. Recently, it has been highlighted that climate models tend to amplify changes of temperature with height in the tropics in warming conditions, following the moist adiabatic lapse-rate (Trenberth and Smith, 2006). The warming and moistening of the troposphere in the experiments performed are accompanied by a constant relative humidity. The result is consistent with the prediction of state of the art GCMs and with radiosonde measurements in the troposphere (Soden et al., 2005). The constraint of a constant relative humidity in a radiative convective equilibrium was suggested by Manabe and Wetherald (1967).

In the present epoch, the ocean surface is colder than the air above only in special locations where cold water is upwelled equatorward and evaporation is inhibited. In our 16xCO2 experiment this condition is extended to all the tropics within 15°S-15°N (fig. 7). A reason for this may be linked to a positive feedback involving clouds. When the CO_2 atmospheric content increases, the induced stability of the troposphere prevents water vapor to rise, inhibiting the convection and reducing the cloud cover fraction (fig. 2b) at high levels. On the contrary, at low levels the cloud cover fraction increases (fig. 2a) preventing a further warming of the SST which remain colder than the air above. The decrease of convective mass flux in a warming climate has been discussed by Held and Soden (2006) and Vecchi and Soden (2007), consistently with the increase in lower tropospheric water vapor, relatively small changes in radiative fluxes and the slowdown of the atmospheric overturning circulation.

Some of the features described suggest a non-linear response of the climate system to the forcing applied. A similar behaviour has been documented by Boer et al. (2005), who performed a set of experiments changing the radiative forcing in the atmosphere by increasing the solar constant. It is nevertheless difficult to relate the two sets of experiments since the radiative forcing perturbations applied in our experiments are not comparable with those used in Boer et al. (2005). Indeed, Boer et al. (2005) increased the solar constant changing the amount of radiation entering the atmosphere, whereas we increased the carbon dioxide concentration in the atmosphere modifying the adjustment processes needed to recover from the imbalance introduced. However, both

the results suggest that there is a threshold in the climate system response where the feedbacks involved are modified, unless the models all lack some mechanisms.

4 Mechanisms involved in the ocean-atmosphere adjustment of the Tropical Pacific sector

As observed in the previous section, the CO_2 rise introduced in the coupled model simulations induces changes in the mean state of the tropical climate. The issue now is to understand the mechanisms of the ocean-atmosphere adjustment responsible of those changes, focusing on the tropical Pacific Ocean.

The heat budget averaged over the global ocean surface is supposed to oscillate around zero if there are no trends in the temperature field. When the initial conditions are strongly perturbed the system is far from the equilibrium, but the adjustment processes push the system toward a constant value. The adjustment time scale is comparable in the 2xCO2 and 4xCO2 experiments but different from the 16xCO2 experiment. At the beginning of the simulation, the more the system is far from the equilibrium the quicker is the adjustment, but then it slows down. In the Equatorial Pacific Ocean the equilibrium of the net surface heat fluxes is reached at a value of 79 W/m^2. In the 2xCO2 and 4xCO2 experiments the adjustment in the equatorial Pacific Ocean is quite rapid and the net heat flux tends to stabilize around the same value of the control experiment. On the other hand, in the 16xCO2 experiment the equilibrium value is smaller than in the other experiments and it is reached after almost 200 years of integration (not shown).

A balanced heat budget at the ocean surface is a constraint for the thermal structure of the ocean. In particular, a decrease in heat loss in the higher latitudes may result in a deepened thermocline (Boccaletti et al., 2004). The mean temperature vertical sections in the Equatorial Pacific Ocean simulated by the coupled model are realistic if compared with the results of an ocean analysis (Masina et al., 2004) (see fig. 9a-b). The simulation in normal CO_2 conditions tends to give colder temperature at the surface and a deeper thermocline in the central-west Pacific. When the CO_2 concentration increases in the atmosphere, the whole upper Equatorial Pacific Ocean warms up (fig. 9 c-e). The warming of the subsurface waters is clearly evident following the changes in the depth of the 20° isotherm (thicker black line in the picture). In the 16xCO2 experiment, the increase of the mean subsurface equatorial temperature in the eastern part of the basin is much larger than in the western part. For instance, at a depth of 150 m the eastern Pacific waters are about 12°C warmer in the 16xCO2 experiment with respect to the control simulation, while in the western basin the difference is of about 8°C.

The zonal average of the net surface heat fluxes in the basin considered is shown in fig. 10. In the 16xCO2 experiment the increase of CO_2 concentration is accompanied by a decrease of the net surface heat flux gained at the Equator and by a decrease of the heat lost in the extra-tropics, mainly in the Northern Hemisphere. In correspondence, the Equatorial Pacific Ocean warms up either at the surface and in the sub-surface and the east-west thermocline slope appears to be reduced in the 16xCO2 experiment. In our experiments we quantify the east-west slope as the difference in thermocline depth between the central and eastern Equatorial Pacific where the depth of the max(dT/dz) is chosen as a proxy of the thermocline depth. Two points in the basin have been chosen (140°W and 110°W) to evaluate the thermocline slope and the results are reported in table 1. Comparing the results of the different CO_2 experiments, the thermocline slope decreases of about 24 m from the control experiment to the 16xCO2 experiment and the isotherms tend to flatten in the central part of the basin as the CO_2 increases (fig. 9).

In the Equatorial Pacific Ocean, from the western up to the eastern side of the basin the SST at the Equator decreases of about 0.4° each 10° of longitude in the control experiment. This gradient tends to weaken as the CO_2 increases until a decrease of 0.2°C each 10° of longitude in the 16xCO2 experiment. The zonal east-west gradient is an important factor for the air-sea coupling (Mechoso et al., 1995). The E-W SST gradient computed as the SST difference between 170°E and 120°W averaged between 2°S and 2°N (Meehl et al., 2001) diminishes when the CO_2 increases (1.4°C in the 16xCO2 experiment compared to 2.9°C of the CTRL).

The thermocline slope is proportional to the forcing of the zonal wind stress across the Equatorial Pacific Ocean (Meehl et al., 2001). In the Tropical Pacific Ocean the simulated zonal wind stress tends to be stronger than observed, mainly along the Equator and in the north (not shown). The annual mean zonal wind stress averaged between 2.5°S and 2.5°N is shown in fig. 11. In the 2xCO2 and 4xCO2 experiments, east of 140°W the increase of the CO_2 concentration produces a modest decrease of the wind, while west of 140°W it is accompanied by a slight intensification of surface winds. In the 16xCO2 experiment the differences with respect to the control experiment become significant and the position of the minimum of mean zonal wind stress is shifted westward with respect to the control experiment. The shift toward west of the surface zonal wind is consistent with the position of the maximum of SST westward with respect to the control simulation. The weakening of the surface zonal wind stress is accompanied by a decrease in the thermocline slope, as found in observations and simplified ocean model's studies (Huang and Pedlosky, 2000; McPhaden and Zhang, 2002; Boccaletti et al., 2004).

Many of the changes previously discussed (e.g. reduction of deep convection, weakening of

surface easterlies and flattening of the thermocline in the Equatorial Pacific Ocean) are consistent with the results found by Vecchi and Soden (2007) comparing the performance of a number of coupled models in the simulation of the mean tropical climate in changing CO_2 scenarios. The consequences of those changes on the Tropical Pacific Ocean variability are discussed in the next section.

5 Impact on the Tropical Pacific interannual variability

The large changes in the mean state caused by increased concentration of carbon dioxide are supposed to affect the variability of tropical Pacific, which is dominated by ENSO. In fact, the equatorial east-west SST gradient, zonal wind stress patterns and thermocline slope are all linked with the El Niño frequency and amplitude.

A measure of the tropical Pacific variability is given by the SST anomalies averaged in the NINO3 (210°-270°E, 5°S-5°N) region. When the CO_2 concentration is increased by a factor of 2 and 4, the standard deviation of the SSTA averaged in the NINO3 area increases (the values are 0.56 in CTRL, 0.60 in 2xCO2 and 0.63 in 4xCO2 experiment), suggesting an increase in the El Niño amplitude. On the other hand, in the 16xCO2 experiment the standard deviation greatly decreases (0.34) with respect to the control experiment, suggesting a weakening of El Niño. Meehl et al. (2001) have shown that models with stronger east-west gradient simulate El Niño with larger amplitudes. In the experiments performed, the E-W SST gradient and the thermocline slope decrease drastically in the 16xCO2 experiment, consistently with the El Niño weakening.

In the control experiment the distribution of monthly SST anomalies in the NINO3 area is almost symmetrical around zero anomaly (not shown). In the 2xCO2 experiment there is an increase in the occurrences of colder events (see also Timmermann et al., 1999). On the other hand in the 16xCO2 experiment the shape of the distribution becomes narrower, with most of the events between -0.5°C and 0.5°C, giving a further evidence of a weakened amplitude.

The El Niño frequency has been correlated to the wind stress anomalies distribution. An equatorial wind stress which shifts westward seems to be associated with an higher frequency El Niño (An and Wang, 2000). A comparison between some coupled models XX century simulations according to IPCC AR4 reveal that all the CGCMs analyzed tend to have zonal wind stress with a meridional scale narrower and centred at a westward longitude than observed, consistently with a simulated ENSO time-scale shorter than observed (Capotondi et al., 2006). A measure of

the wind stress shift is given by the centre of mass defined as

$$C = \frac{\int_0^{L_x} \tau^x(x) x dx}{\int_0^{L_x} \tau^x dx} \tag{1}$$

when τ^x are the zonal wind stress anomalies regressed upon the NINO3.4 index and L_x is the length of the basin at the Equator (Capotondi et al., 2006). In the CO_2 experiments the computed C moves westward with respect to the control experiment, suggesting an high-frequency ENSO (fig. 12, where the position of the centre of mass is represented by a solid line). The NINO3.4 index is the average of monthly mean SST in the area 5°S-5°N, 170°-120°W.

To measure the frequency of ENSO it is appropriate to compute the power spectra of the NINO3 index (fig. 13, where each panel contains the power spectrum density (PSD) for each CO_2 experiment within 99% confidence intervals). In the control experiment, the PSD has two dominant peaks, one at 2 years and an other at about 3 years (fig. 13a). In the 2xCO2 and 4xCO2 experiments the dominant peak becomes a broad spectrum that maximizes around 2-3 years (fig. 13b,c). The ordinate scale for the CTRL spectrum differs from the CO_2 experiments because when the CO_2 concentration increases the maximum of the PSD decreases. In fact, in the 16xCO2 experiment (fig. 13d) the maximum of the PSD is drastically reduced and from the distribution of the peaks it is hard to identify a dominant frequency at interannual timescale. The decrease in the dominant frequency is so severe in the 16xCO2 case that is very suggestive of a practical collapse of the interannual variability.

The changes observed in the mean state and described in section 3, as well as the discussion of section 4, about the mechanisms involved, suggest the conclusion that a world with high carbon dioxide concentration produce a mean state with some characteristics which suggest the establishment of permanent warm conditions that look like the peak of El Niño (e.g. the reduction of the east-west temperature gradient, the weakening of the easterlies and the flattening of the thermocline in the Equatorial Pacific Ocean).

6 Conclusions

The concept of climate sensitivity assumes that climate response is approximately proportional to radiative forcing, but yet not much is known about the range of forcing under which such a view is reasonable. In fact, the response of the climate system to strong forcing is still under debate. Understanding the main processes involved in strong forcing regimes might lead to interesting paleoclimate applications.

The ocean-atmosphere adjustment in extreme CO_2 conditions has been studied by means of sensitivity experiments integrated with a coupled general circulation model with interactive ice. The motivation that inspired this study is the understanding of the adjustment processes in extreme CO_2 conditions and not the simulation of the climate under realistic future scenarios. The starting idea of this study is that a strong perturbation in the heat fluxes may induce large changes at the ocean-atmosphere interface, as well as in the thermal structure of the ocean and the troposphere. In this context, a control simulation experiment with present-day values of carbon dioxide concentration has been compared with experiments in which the CO_2 concentration has been multiplied by a factor of 2, 4 and 16.

The annual mean state simulated in extreme CO_2 conditions is characterized by a general warming of both ocean and atmospheric temperatures. The 16xCO2 simulation exhibits a particularly large response. The normal unstable condition with the ocean surface warmer than the air above, which is a requisite for convection to occur, changes to a mean state with the ocean surface colder than the air above in the tropical band of both Pacific and Indian Oceans. In those conditions, the atmosphere is more stable and the convection is suppressed: the mean total precipitation appears to be the result of large-scale moisture flux even in the tropics. The increased stability of the surface is accompanied by a more stable troposphere even at higher levels. The vertical profile of the atmospheric temperature is indeed characterized by an enhanced warming in the upper troposphere in the sensitivity experiments with respect to the control simulation. The stability of the upper troposphere is accompanied by a decrease in the high level clouds and an increase at low levels which prevents SST to further warm keeping them colder than the air above.

In the ocean, both surface and sub-surface waters are warmer than in the control simulation. The eastern and western sides of the tropical Pacific Ocean behave differently. At the surface, the zonal SST gradient between eastern and western Pacific Ocean decreases, up to 50% in the 16xCO2 experiment compared to the control experiment. Similarly, in the sub-surface the eastern waters warm more than the western one as the warming extends deep in the ocean (for instance the 20°C isotherm lies below 200 m) preventing cold waters to upwell in the east. The thermocline slope in the 16xCO2 experiment decreases of about 24 m with respect to the control simulation, consistently with a decreased surface zonal wind stress.

The analysis of the interannual variability in the Eastern Equatorial Pacific Ocean by means of the NINO3 SSTA index shows that, in the experiments where the CO_2 concentration is increased by a factor of 2 and 4, there is an increase of the standard deviation of the index up to 12%. On the other hand, in the experiment where the CO_2 concentration is increased by a factor of 16

the standard deviation of the NINO3 index decreases of about 40% with respect to the control experiment, suggesting a weakening of the tropical variability.

The changes in the characteristics of El Niño together with the analysis of the mean state of the ocean in the Tropical Pacific sector suggest the possibility of the establishment of permanent warm conditions that look like the peak of El Niño, with weaker easterly winds, smaller temperature gradient at the Equator between the eastern and western Pacific Ocean and a flatter thermocline. Similar permanent warm conditions were present approximately three million years ago, even if in that period the CO_2 concentration was similar to present-day value (Fedorov et al., 2006). One of the mechanisms discussed by Fedorov et al. (2006) to explain the Pliocene warm conditions imply a reduced poleward heat transport associated with a sufficient large freshening in the extra-tropics. Our findings are in line with those results as we observed a smaller globally averaged ocean heat transport and a decreased heat loss at high latitudes. Nevertheless, the fact that we obtained Pliocene similar permanent warm conditions in the tropics with a much higher CO_2 concentration suggest the possibility that the state of the art coupled models might miss some important feedbacks and are not yet able to reproduce a climate state similar to the one present during the Pliocene.

The results of this study reveal a non-linear sensitivity of the dynamics in the tropical and extra-tropical regions to the increase in the carbon dioxide concentration imposed in the analyzed experiments. The correspondence between our results and previous findings (e.g. Boer et al., 2005; Vecchi and Soden, 2007) is not enough to exclude the possibility of a dependence on the parameterizations implemented within the model used (e.g. convection and radiation schemes). Increased low cloud cover with increased CO_2 concentration has been associated to an increased stability of the lower troposphere, in agreement with previous analysis (Vecchi and Soden, 2007). Nevertheless, cloud cover schemes are still the largest source of uncertainty in current climate models (Soden and Held, 2006).

Acknowledgements. We thank the European Community project DYNAMITE, contract 003903-GOCE, for the financial support. We are grateful to S. Gualdi, E. Scoccimarro and all the INGV people involved in the coupling of the SINTEXG model. Particularly, we thank the two anonymous reviewers whose suggestions and constructive criticism have significantly improved the manuscript.

References

An S-I, Wang B (2000) Interdecadal change of the structure of the ENSO mode and its impact on the ENSO frequency. J Clim 13: 2044–2055

Blanke B, Delecluse P (1993) Low frequency variability of the tropical Atlantic ocean simulated by a General Circulation Model with mixed-layer physics. J Phys Oceanogr 23: 1363–1388

Boccaletti G, Pakanowski RC, Philander SGH (2004) The thermal structure of the upper ocean. J Phys Oceanogr 34: 888–902

Boer GJ, Hamilton K, Zhu W (2005) Climate sensitivity and climate change under strong forcing. Clim Dyn 24: 685-700

Capotondi A, Wittenberg A, Masina S (2006) Spatial and temporal structure of Tropical Pacific interannual variability in 20th century coupled simulations. Oc Model 15: 274–298

Clement AC, Seager R, Cane MA, Zebiak SE (1996) An ocean dynamical thermostat. J Clim 9: 2190–2196.

Collins M (2000) The El Niño Southern Oscillation in the second Hadley Center coupled model and its response to greenhouse warming. J Clim 13: 1299–1312

Da Silva A, Young AC, Levitus S (1994) Atlas of Surface Marine Data 1994, Volume 1: Algorithms and Procedures. NOAA Atlas NESDIS 6, U.S. Department of Commerce, Washington, D.C.

Fedorov AV, Dekens PS, McCarthy M, Ravelo AC, deMenocal PB, Barreiro M, Pacanowski RC, Philander SGH (2006) The Pliocene Paradox (Mechanisms for a permanent El Niño). Science 312: 1485–1489

Fichefet T, Morales Maqueda MA (1999) Modelling the influence of snow accumulation and snow-ice formation on the seasonal cycle of the Antarctic sea-ice cover. Clim Dyn 15: 251–268

Gualdi S, Scoccimarro E, Navarra A (2007) Changes in Tropical Cyclone Activity due to Global Warming: Results from a High-Resolution Coupled General Circulation Model. Submitted to J Clim

Gualdi S, Navarra A, Guilyardi E, Delecluse P (2003) Assessment of the tropical Indo-Pacific climate in the SINTEX CGCM. Ann Geophys 46: 1–26

Guilyardi E (2006) El Ni no-mean state-seasonal cycle interactions in a multi-model ensemble. Clim Dyn 26: 329–348

Guilyardi E, Delecluse P, Gualdi S, Navarra A (2003) Mechanisms for ENSO phase change in a coupled GCM. J Clim 16: 1141–1158

Held IM, Soden BJ (2006) Robust responses of the hydrological cycle to global warming. J Clim 19: 5686–5699

Houghton JT, Ding Y, Griggs DJ, Noguer M, van der Linden PJ, Xiaosu D, Eds (2001) Climate Change 2001: The scientific basis. Contribution of Working Group I to the Third Assessment Report of the Intergovernmental Panel on Climate Change. Cambridge University Press, 881 pp.

Huang RX, Pedlosky J (2000) Climate variability of the equatorial thermocline inferred from a two-moving-layer model of the ventilated thermocline. J Phys Oceanogr 30: 2610–2626

IPCC, 2001: *Climate Change 2001. The scientific basis*. Eds. Houghton JT, Ding Y, Nogua M, Griggs D,

Vander Linden P, Maskell K, Cambridge Univ Press, Cambridge, U.K.

IPCC, 1995: *The Science of Climate Change*, Cambridge University Press, 572 pp.

Knutson TR, Manabe S (1995) Time-mean response over the tropical Pacific to increased CO_2 in a coupled ocean-atmosphere model. J Clim 8: 2181–2199

Liu Z, Vavrus S, He F, Wen N, Zhong Y (2005) Rethinking tropical ocean response to global warming: The enhanced equatorial warming. J Clim 18: 4684–4700

Madec G, Delecluse P, Imbard M, Levy C (1998) OPA version 8.1 Ocean General Circulation Model reference manual. Tech Rep LODYC/IPSL Note 11

Manabe S, Wetherald RT (1967) Thermal equilibrium of the atmosphere with a given distribution of relative humidity. J Atmos Sci 24: 241–259

Masina S, Di Pietro P, Navarra A (2004) Interannual-to-decadal variability of the North Atlantic from an ocean data assimilation system. Clim Dyn 23: 531–546

McPhaden MJ, Zhang D (2002) Slowdown of the meridional overturning circulation in the upper Pacific Ocean. Nature 415: 603–608

Mechoso CR, Robertson AW, Barth N, Davey MK, Delecluse P, Gent PR, Ineson S, Kirtman B, Latif M, LeTreut H, Nagal T, Neelin JD, Philander SGH, Polcher J, Schopf PS, Stockdale T, Suarez MJ, Terray L, Thual O, Tribbia JJ (1995) The seasonal cycle over the tropical Pacific in coupled ocean-atmosphere general circulation models. Mon Weather Rev 123: 2825–2838

Meehl GA, Teng H, Branstator G (2006) Future changes of El Niño in two global coupled models. Clim Dyn 26(6): 549–566

Meehl GA, Gent P, Arblaster JM, Otto-Bliesner B, Brady E, Craig A (2001) Factors that affect amplitude of El Niño in global coupled climate models. Clim Dyn 17: 515–526

Merryfield WJ (2006) Changes to ENSO under CO_2 doubling in a multi-model ensemble. J Clim 19: 4009–4027

Pierrehumbert RT (1995) Thermostats, radiator fins and the local runaway greenhouse. J Atmos Sci 52(10): 1784–1806

Ramanathan V, Collins W (1992) Thermostat and global warming. Nature 357: 649

Ramanathan V, Collins W (1991) Thermodynamic regulation of ocean warming by cirrus clouds deduced from observations of the 1987 El Niño. Nature 351: 27–32

Rayner NA, Parker DE, Horton EB, Folland CK, Alexander LV, Rowell DP, Kent EC, Kaplan A (2003) Global analysis of sea surface temperature, sea ice and night marine air temperature since the late nineteenth century. J Geophys Res 18(D14) 4407 doi:10.1029/2002JD002670

Roeckner E, Arpe K, Bengtsson L, Christoph M, Claussen M, Dümenil L, Esch M, Giorgetta M, Schlese U, Schulzweida U (1996) The Atmospheric general circulation Model ECHAM4: Model description and simulation of present-day climate. *Max-Planck Institut für Meteorologie*, Report no. 218, Hamburg, 86 pp.

Soden BJ, Held IM (2006) An assessment of climate feedbacks in coupled ocean-atmosphere models. J

Clim 19: 3354–3360

Soden BJ, Jackson DL, Ramaswamy V, Schwarzkopf MD, Huang X (2005) The radiative signature of upper tropospheric warming. Science 310: 841–844

Timmermann A, Oberhuber J, Bacher A, Esch M, Latif M, Roeckner E (1999) Increased El Niño frequency in a climate model forced by future greenhouse warming. Nature 398: 694–696

Trenberth KE, Smith L (2006) The vertical structure of temperature in the Tropics: Different flavours of El Niño. J Clim 19: 4956–4970

Trenberth KE, Jones PD, Ambenje P, Bojariu R, Easterling D, Klein Tank A, Parker D, Rahimzadeh F, Renwick JA, Rusticucci M, Soden BJ, Zhai P (2007) Observations: surface and atmospheric climate change. In: *Climate Change 2007: The physical science basis*. Contribution of Working Group I to the Fourth Assessment Report of the Intergovernmental Panel on Climate Change [Solomon S, Qin D, Manning M, Chen Z, Marquis M, Averyt KB, Tignor M, Miller HL (eds.)]. Cambridge University Press, Cambridge, United Kingdom and New York, NY, USA.

Valcke S, Terray L, Piacentini A (2000) The Oasis coupler user guide version 2.4. Tech Rep TR/CMGC/00-10, CERFACS.

Vecchi GA, Soden BJ (2007) Global warming and the weakening of the tropical circulation. J Clim 20: 4316–4340

Vecchi GA, Soden BJ, Wittenberg AT, Held IM, Leetma A, Harrison MJ (2006) Weakening of tropical Pacific atmospheric circulation due to anthropogenic forcing. Nature 441: 73–76

Wallace JM (1992) Effect of deep convection on the regulation of tropical sea surface temperature. Nature 357: 230–231.

Zhang GJ, McPhaden MJ (1995) The relationship between sea surface temperature and latent heat flux in the Equatorial Pacific. J Clim 8: 589–605.

Tables

	CTRL	**2 × CO2**	**4 × CO2**	**16 × CO2**
110°W	65	65	65	45
140°W	129	129	117	85
140°W minus 110°W	64	64	52	40

Table 1. Depth (m) of the maximum of dT/dz at 110°W and 140°W in the Equatorial (2.5°S and 2.5°N) Pacific Ocean.

Figure Captions

Fig. 1. Annual mean net surface heat flux (W/m^2), computed as SWR (Short Wave Radiation) + LWR (Long Wave Radiation) + SHF (Sensible Heat Flux) + LHF (Latent Heat Flux), for the observations (a) and the control experiment (b). Annual mean net surface heat fluxes differences (W/m^2): 2xCO2-CTRL (c), 4xCO2-CTRL (d), 16xCO2-CTRL (e). The thick black line in all the panels is the 0 contour.

Fig. 2. Annual mean of zonally averaged cloud cover fraction at (a) 850 mb and (b) 150 mb for CTRL and CO_2 experiments (see legend within each panel).

Fig. 3. Annual zonal mean net surface heat flux (W/m^2) averaged over the global ocean (a) and SST (b). Global ocean heat transport (c) and global atmosphere heat transport (d) in CTRL and CO_2 experiments (see legend within each panel). SST is measured in $^\circ$C and heat transports in PW. The global atmosphere heat transport is computed as $[\overline{vT}]$ where the square brackets refer to the zonal average, while the overbar indicates the time mean.

Fig. 4. Annual mean sea surface temperature ($^\circ$C) in the HadISST dataset (a) and in the CTRL experiment (b). Panels in the right report the differences with respect to the CTRL of (c) 2xCO2, (d) 4xCO2 and (e) 16xCO2 experiments. In the right panels the differences have been scaled to the global mean difference reported in the top of each panel. The negative values do not correspond to a cooling but to the departure of the differences from the global mean difference with respect to the CTRL experiment. The thick black line in the right panels is the 0 contour.

Fig. 5. Annual mean total precipitation (mm/day) in the control experiment (a). Differences from CTRL in (b) 2xCO2, (c) 4xCO2 and (d) 16xCO2 experiments.

Fig. 6. Annual mean convective precipitation (mm/day) in the CTRL experiment (a). Differences from the CTRL in (b) 2xCO2, (c) 4xCO2 and (d) 16xCO2 experiments.

Fig. 7. Annual mean SST minus temperature at 2 m ($^\circ$C) averaged in the 15°S-15°N band in CTRL and CO_2 experiments (see legend within the picture).

Fig. 8. Annual mean atmospheric temperature in the Tropical (averaged between 15°S and 15°N) Pacific Ocean in CTRL and CO_2 experiments (see legend within the picture).

Fig. 9. Annual mean of temperature sections (°C) in the Equatorial (between 2.5°S and 2.5°N) Pacific Ocean for (a) the ocean analysis, (b) CTRL, (c) 2xCO2, (d) 4xCO2 and (e) 16xCO2 experiment.

Fig. 10. Annual mean net surface heat flux (W/m^2) averaged in the Pacific Ocean for CTRL and CO_2 experiments (see legend within the picture).

Fig. 11. Annual mean zonal wind stress (N/m^2) averaged in the Equatorial (2.5°-2.5°N) Pacific Ocean for CTRL and CO_2 experiments (see legend within the picture).

Fig. 12. Zonal wind stress monthly mean anomalies regressed upon the NINO3.4 index (10^{-3} Pa/°C) in the control experiment (a), 2xCO2 experiment (b), 4xCO2 experiment (c) and 16xCO2 experiment (d). The thick black line indicates the longitude of the centre of mass (see definition in the text), which exact position is specified in the bottom of the corresponding panel.

Fig. 13. Power spectrum density (PSD) of monthly mean NINO3 SST for CTRL (a), 2xCO2 (b), 4xCO2 (c) and 16xCO2 (d) experiments. The PSD is computed by means of the Thomson multitaper method and the 99% confidence intervals of each spectrum (thin lines) computed through a chi-square approach are included in each panel. The dashed line corresponds to the PSD of a first order auto-regressive model fitted on the data. The peaks above the dashed line are indicative of a difference from a red-noise process.

Figures

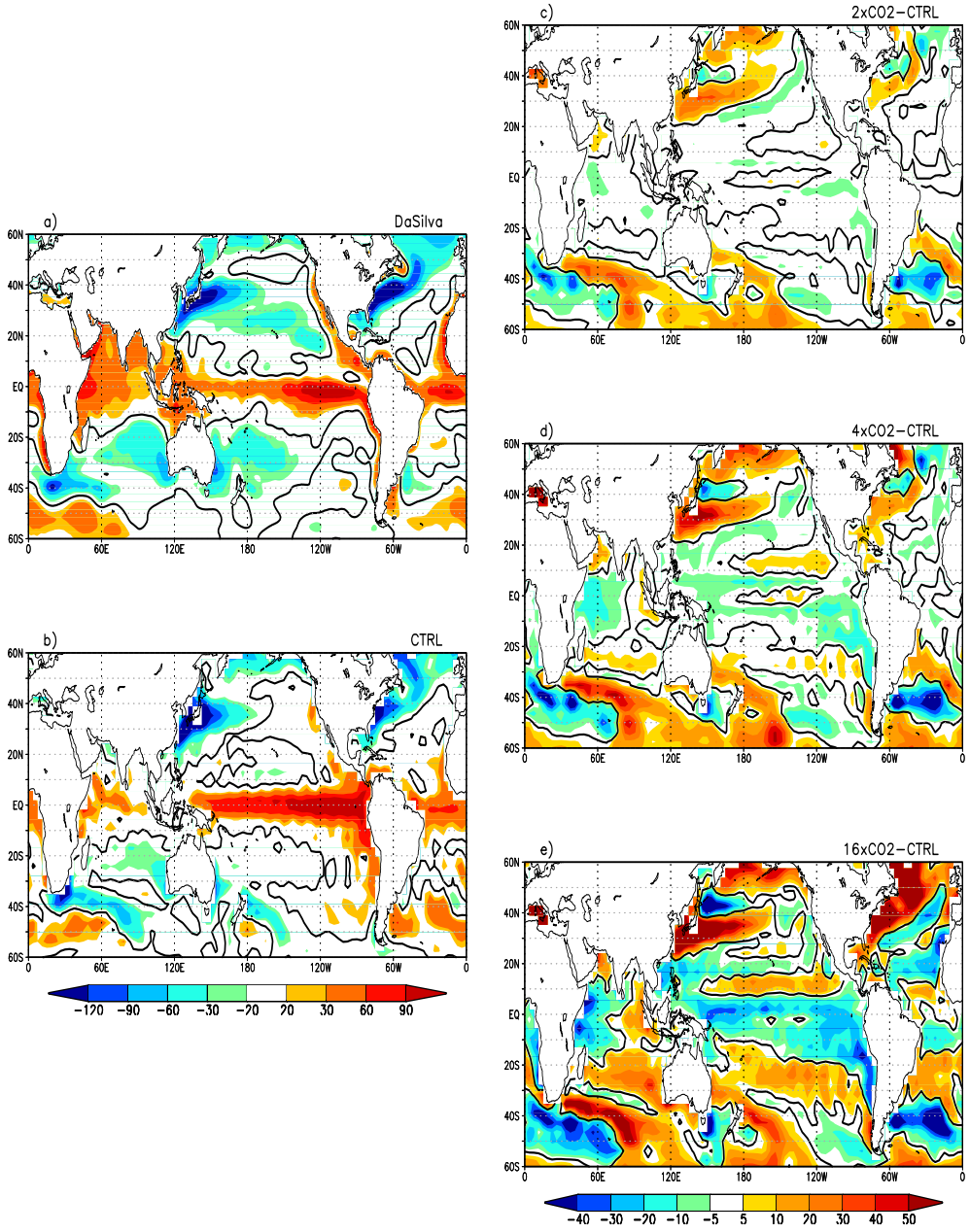

Fig. 1. Annual mean net surface heat flux (W/m^2), computed as SWR (Short Wave Radiation) + LWR (Long Wave Radiation) + SHF (Sensible Heat Flux) + LHF (Latent Heat Flux), for the observations (a) and the control experiment (b). Annual mean net surface heat fluxes differences (W/m^2): 2xCO2-CTRL (c), 4xCO2-CTRL (d), 16xCO2-CTRL (e). The thick black line in all the panels is the 0 contour.

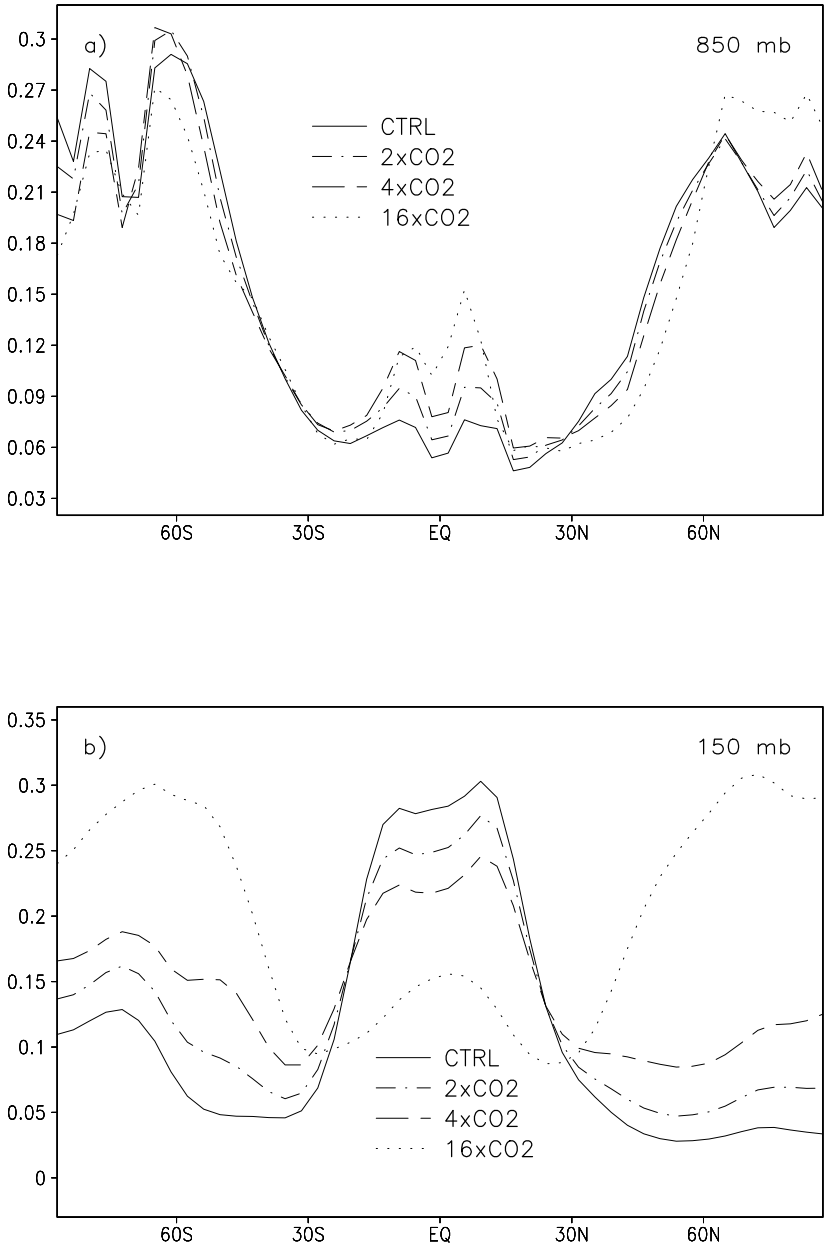

Fig. 2. Annual mean of zonally averaged cloud cover fraction at (a) 850 mb and (b) 150 mb for CTRL and CO_2 experiments (see legend within each panel).

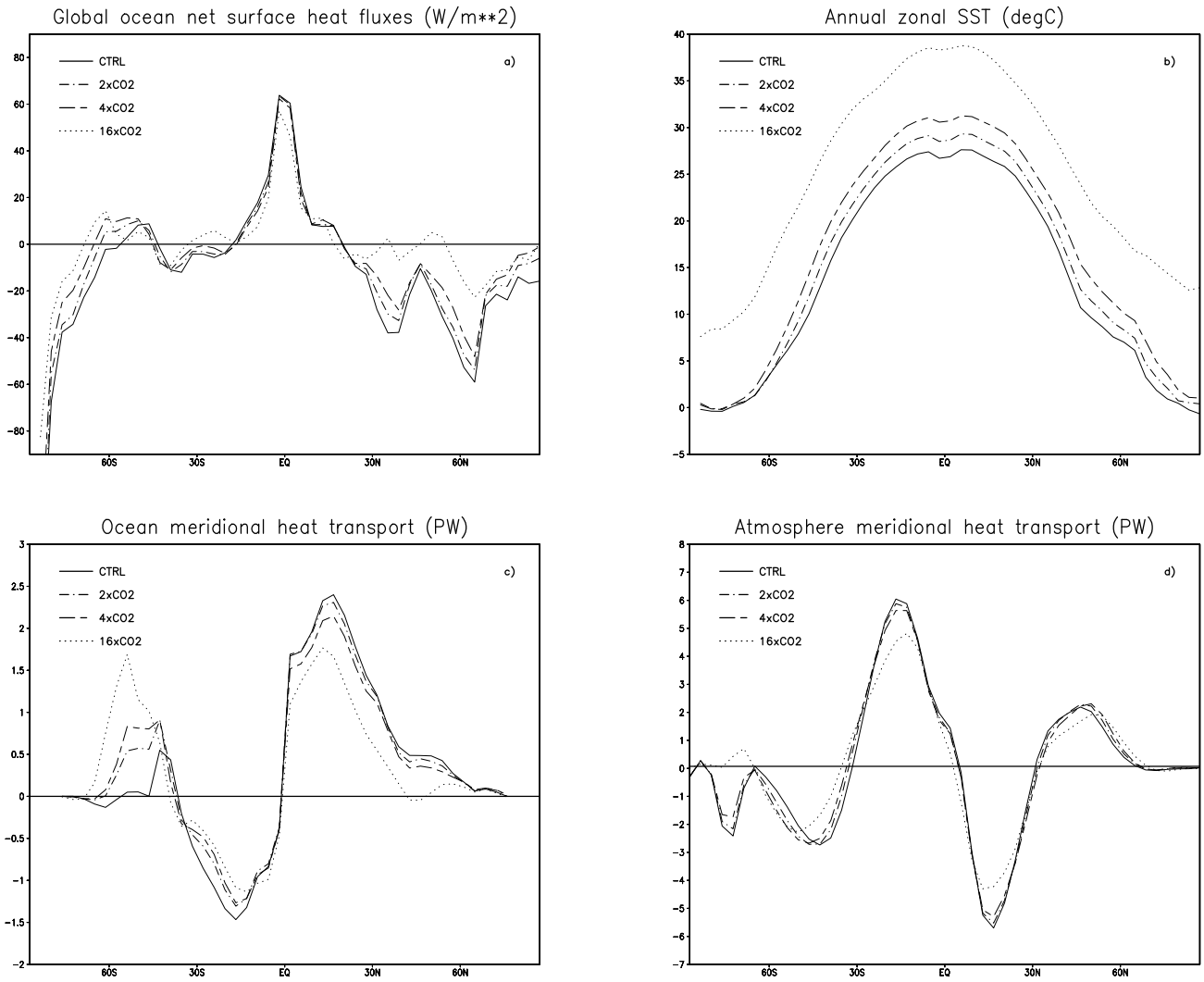

Fig. 3. Annual zonal mean net surface heat flux ($\mathrm{W/m^2}$) averaged over the global ocean (a) and SST (b). Global ocean heat transport (c) and global atmosphere heat transport (d) in CTRL and CO_2 experiments (see legend within each panel). SST is measured in $^\circ$C and heat transports in PW. The global atmosphere heat transport is computed as $[\overline{\mathrm{vT}}]$ where the square brackets refer to the zonal average, while the overbar indicates the time mean.

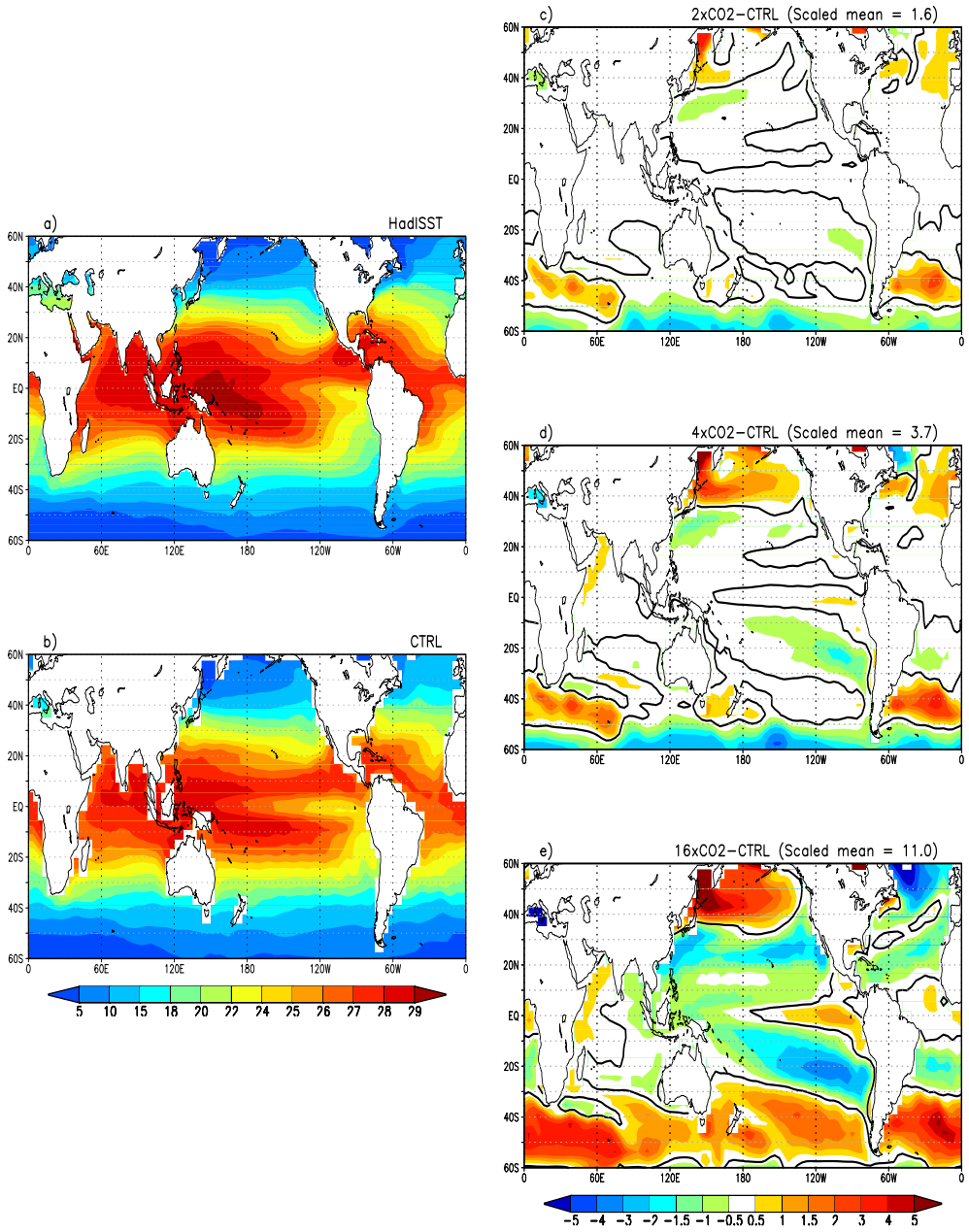

Fig. 4. Annual mean sea surface temperature (°C) in the HadISST dataset (a) and in the CTRL experiment (b). Panels in the right report the differences with respect to the CTRL of (c) 2xCO2, (d) 4xCO2 and (e) 16xCO2 experiments. In the right panels the differences have been scaled to the global mean difference reported in the top of each panel. The negative values do not correspond to a cooling but to the departure of the differences from the global mean difference with respect to the CTRL experiment. The thick black line in the right panels is the 0 contour.

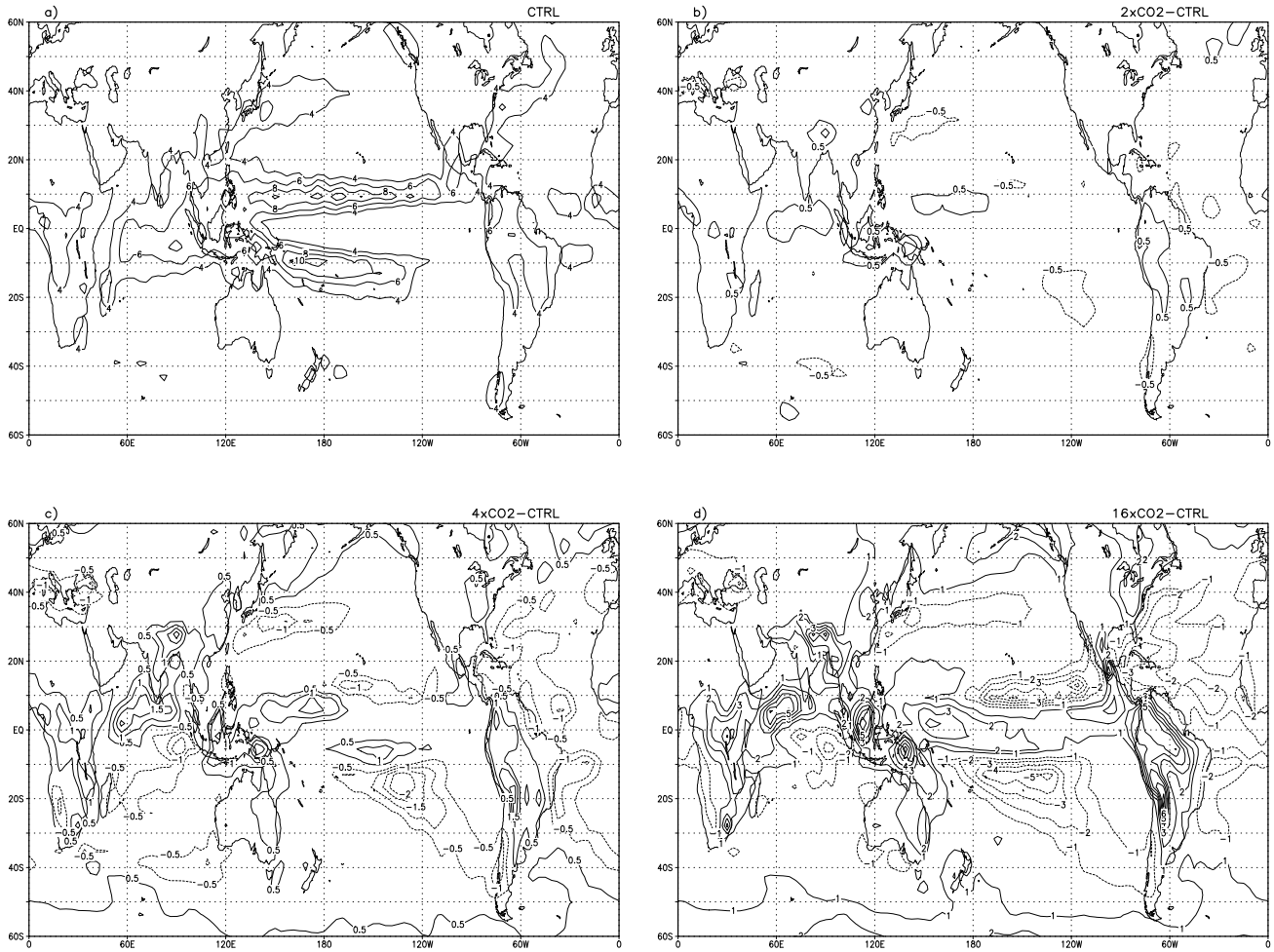

Fig. 5. Annual mean total precipitation (mm/day) in the control experiment (a). Differences from CTRL in (b) 2xCO2, (c) 4xCO2 and (d) 16xCO2 experiments.

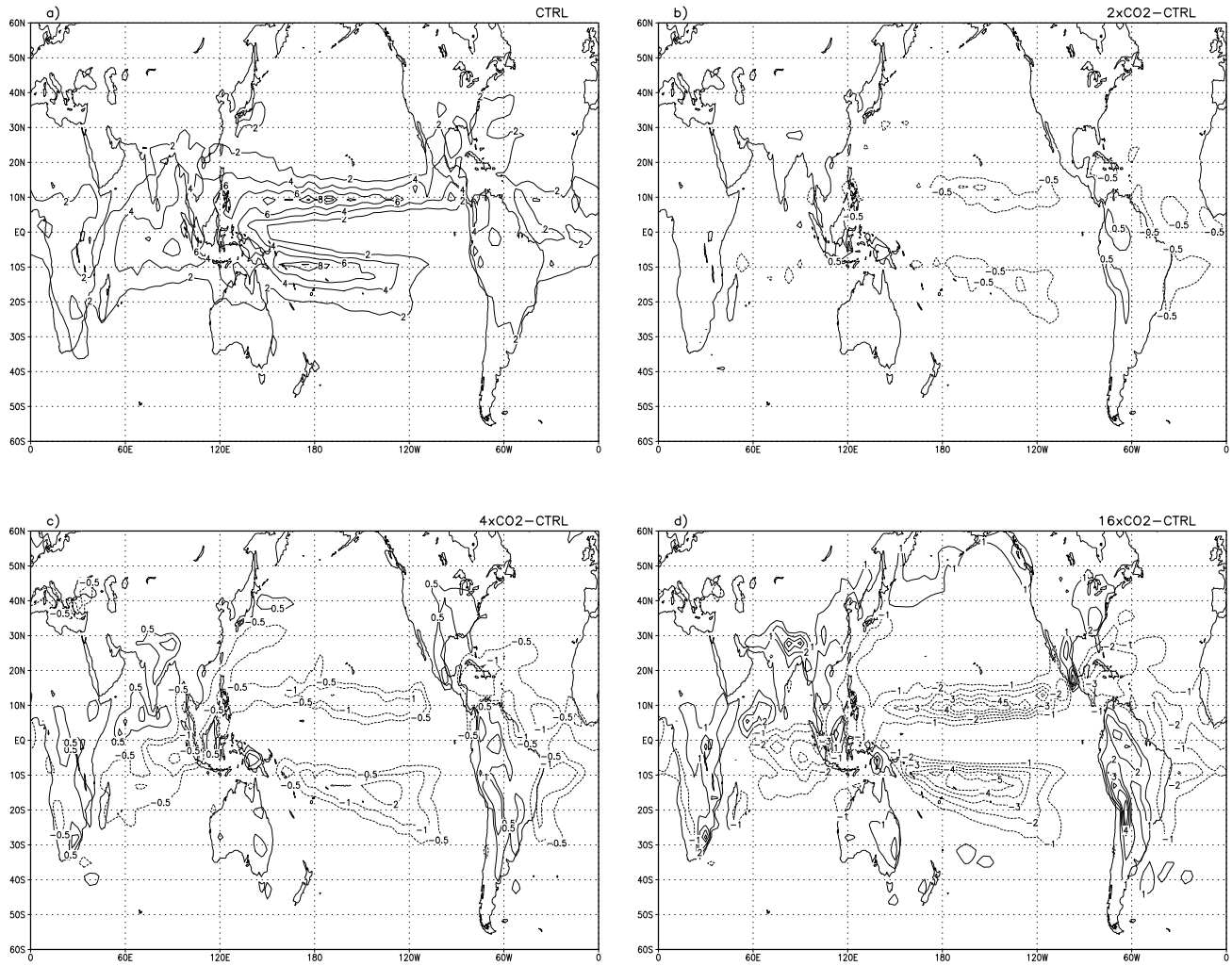

Fig. 6. Annual mean convective precipitation (mm/day) in the CTRL experiment (a). Differences from the CTRL in (b) 2xCO2, (c) 4xCO2 and (d) 16xCO2 experiments.

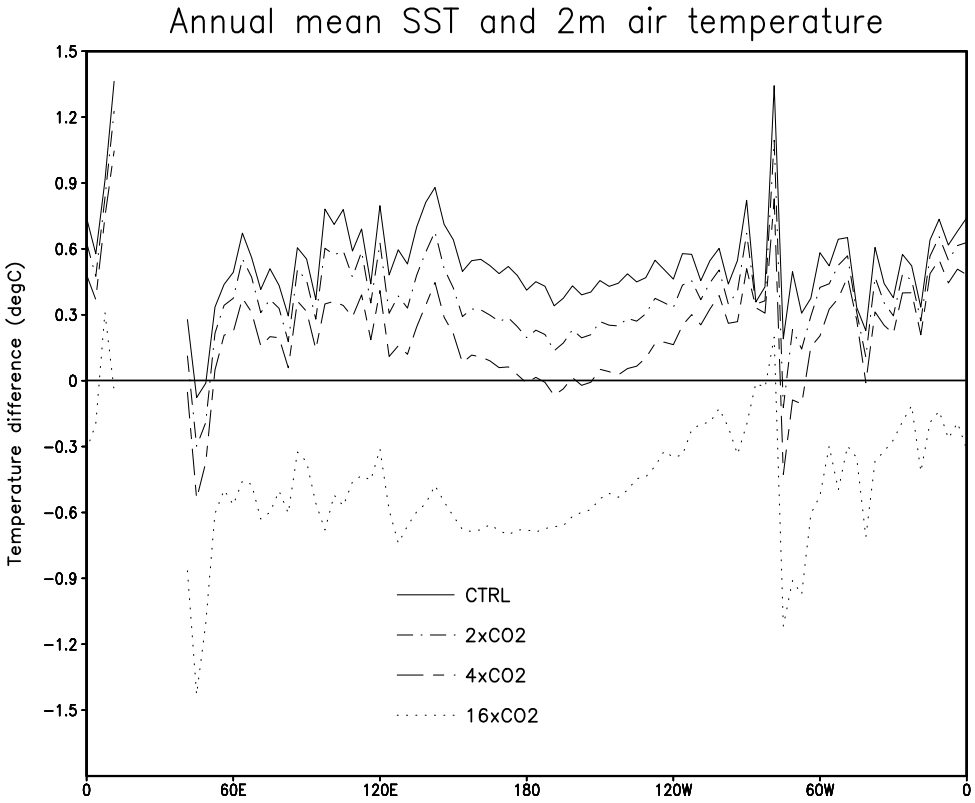

Fig. 7. Annual mean SST minus temperature at 2 m (°C) averaged in the 15°S-15°N band in CTRL and CO_2 experiments (see legend within the picture).

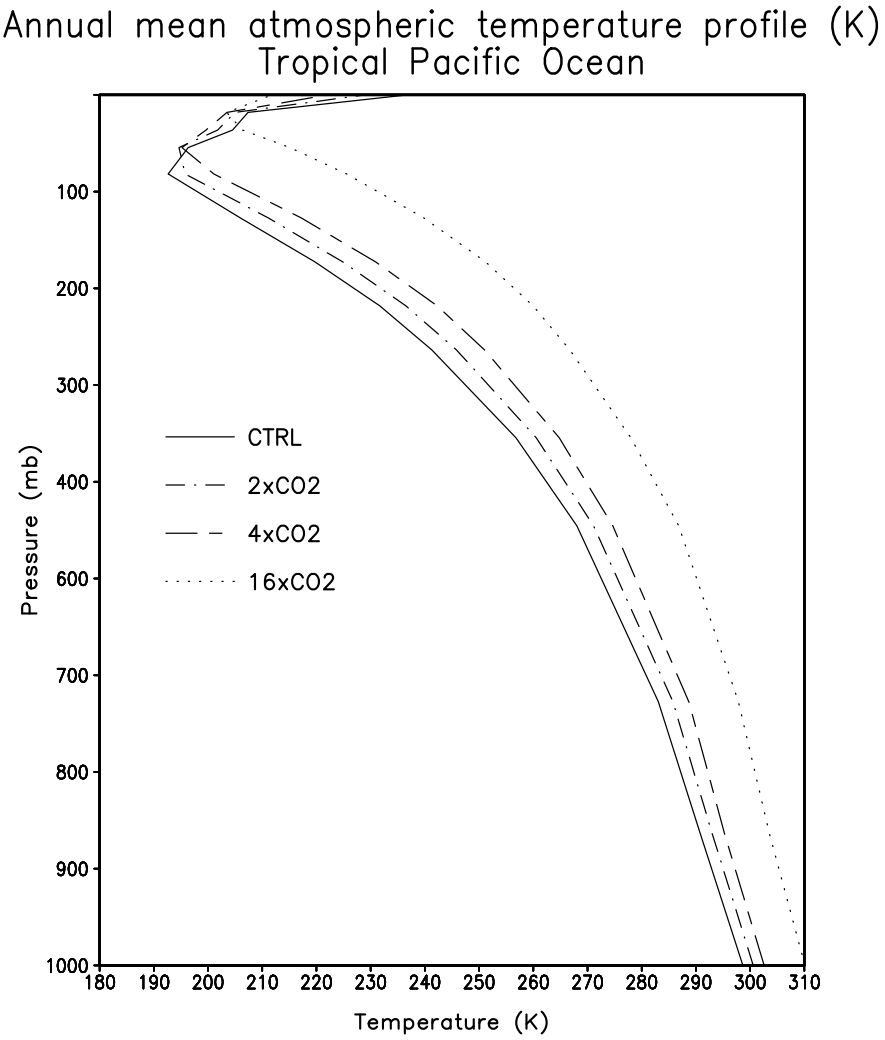

Fig. 8. Annual mean atmospheric temperature in the Tropical (averaged between 15°S and 15°N) Pacific Ocean in CTRL and CO_2 experiments (see legend within the picture).

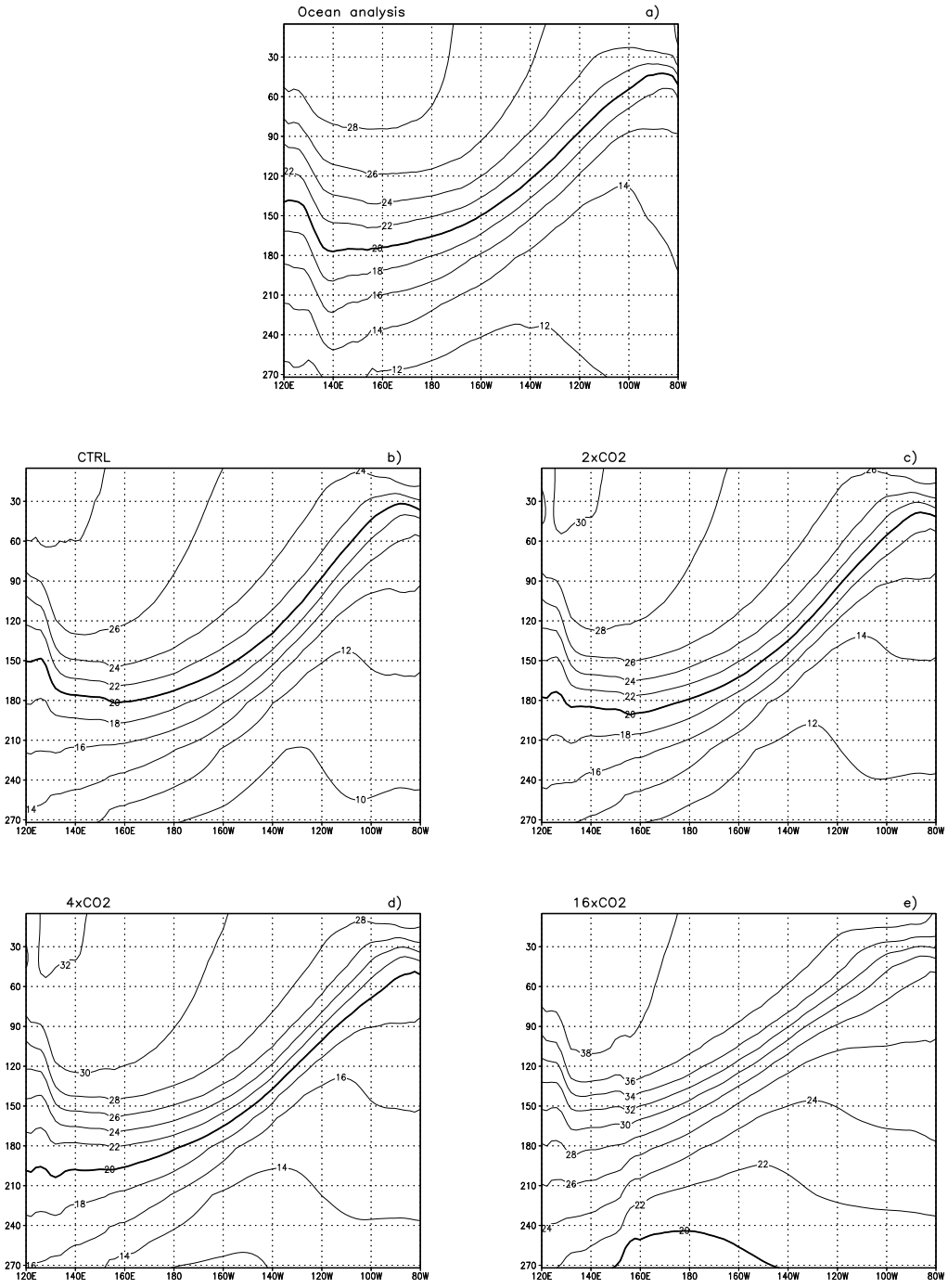

Fig. 9. Annual mean of temperature sections (°C) in the Equatorial (between 2.5°S and 2.5°N) Pacific Ocean for (a) the ocean analysis, (b) CTRL, (c) 2xCO2, (d) 4xCO2 and (e) 16xCO2 experiment.

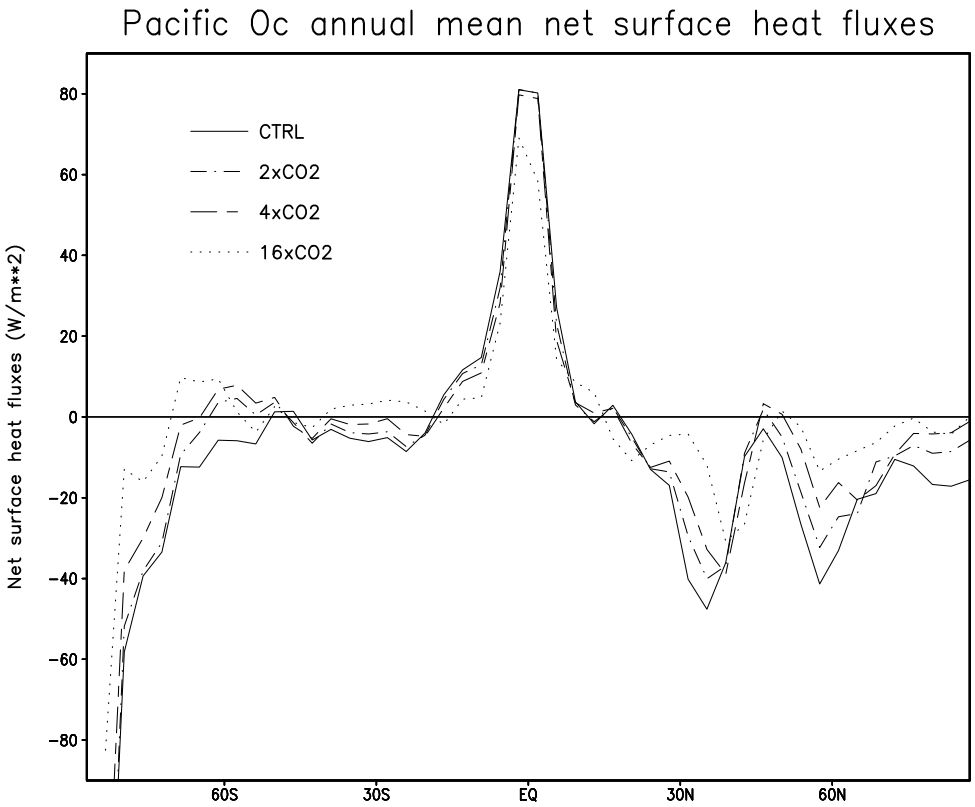

Fig. 10. Annual mean net surface heat flux (W/m^2) averaged in the Pacific Ocean for CTRL and CO_2 experiments (see legend within the picture).

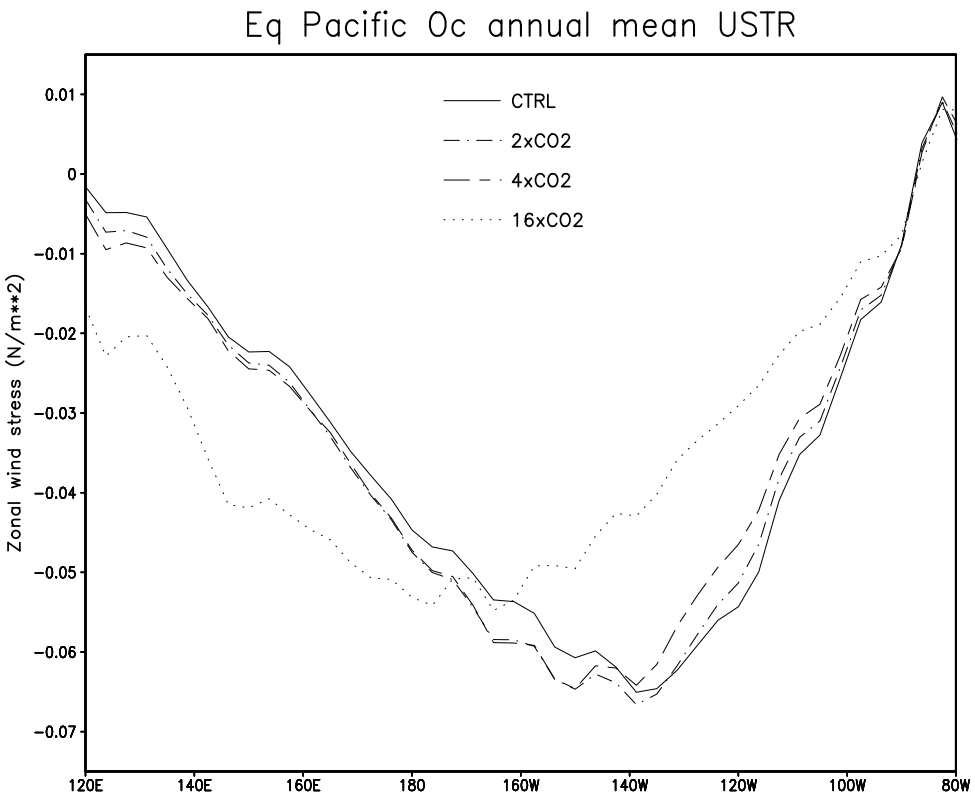

Fig. 11. Annual mean zonal wind stress (N/m^2) averaged in the Equatorial (2.5°-2.5°N) Pacific Ocean for CTRL and CO_2 experiments (see legend within the picture).

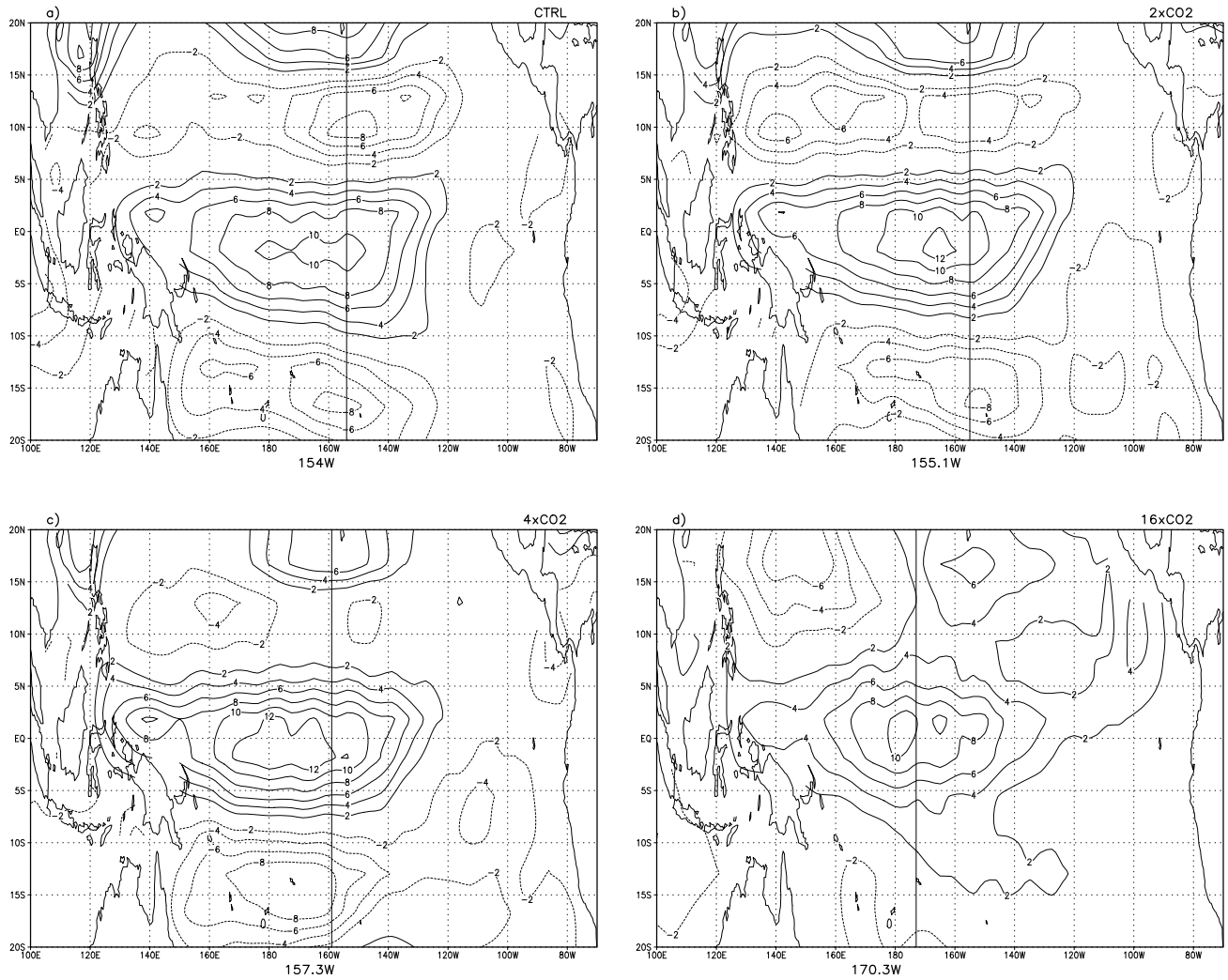

Fig. 12. Zonal wind stress monthly mean anomalies regressed upon the NINO3.4 index (10^{-3} Pa/°C) in the control experiment (a), 2xCO2 experiment (b), 4xCO2 experiment (c) and 16xCO2 experiment (d). The thick black line indicates the longitude of the centre of mass (see definition in the text), which exact position is specified in the bottom of the corresponding panel.

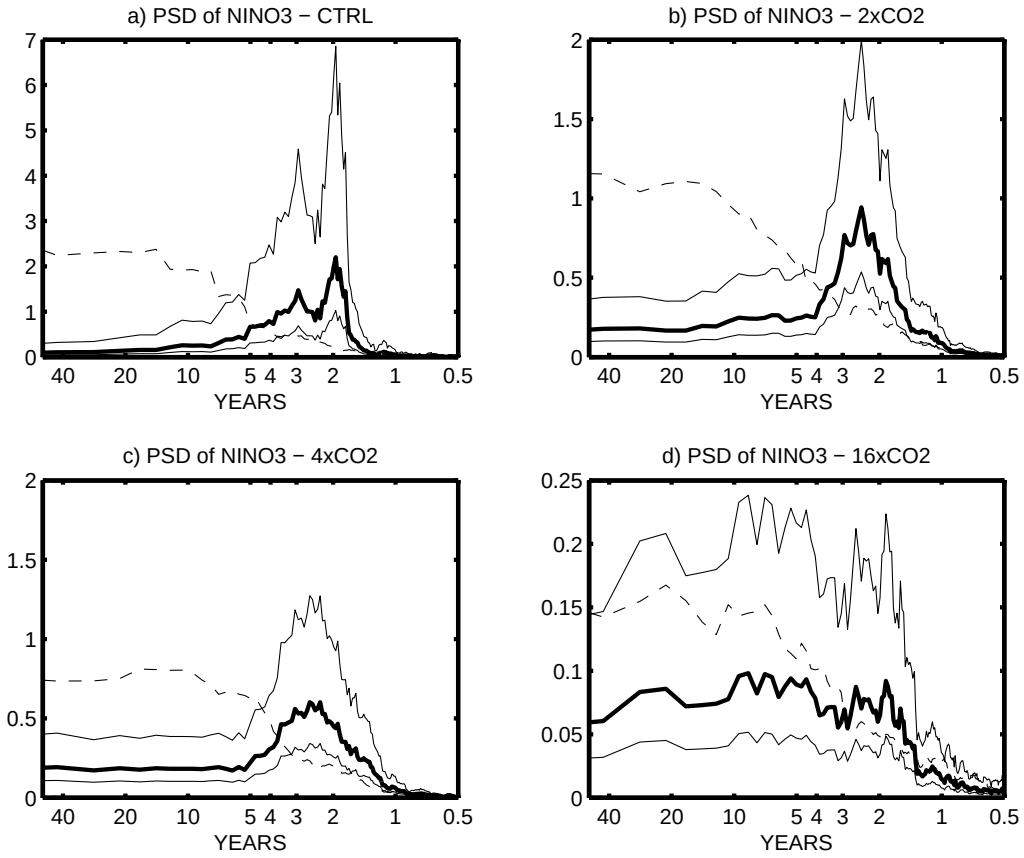

Fig. 13. Power spectrum density (PSD) of monthly mean NINO3 SST for CTRL (a), 2xCO2 (b), 4xCO2 (c) and 16xCO2 (d) experiments. The PSD is computed by means of the Thomson multitaper method and the 99% confidence intervals of each spectrum (thin lines) computed through a chi-square approach are included in each panel. The dashed line corresponds to the PSD of a first order auto-regressive model fitted on the data. The peaks above the dashed line are indicative of a difference from a red-noise process.